Water Science & Technology

IWA PUBLISHING

Water Science & Technology Vol 84 No 5, 1228 doi: 10.2166/wst.2021.315

TiO_2 and carbon nanotubes composites modify capacitive deionization anodes to improve the dechlorination efficiency in desulfurization wastewater

Shuangchen Ma[a,b,*], Chang Liu[a,b], Yongyi Xu[c], Yu Tan[a], Dingchang Yang[a], Feng Wang[c] and Lan Ma[a,b]

[a] Hebei Key Laboratory of Power Plant Flue Gas Multi-Pollutants Control, Department of Environmental, Science and Engineering, North China Electric Power University, Baoding 071003, China
[b] MOE Key Laboratory of Resources and Environmental Systems Optimization, Beijing 102206, China
[c] China Power Hua Chuang Electricity Technology Research Company Ltd, Suzhou 215000, China
*Corresponding author. E-mail: msc1225@163.com

ABSTRACT

A new capacitive deionization (CDI) technology was used to remove Cl^- from desulfurization wastewater. TiO_2 and carbon nanotubes (CNTs) were combined with N-methyl pyrrolidone (NMP) to form composites by a solvothermal method in which it is coated onto the CDI anode to improve dechlorination efficiency (DE). The morphology, surface area, wettability, crystal structure and chemical composition of the TiO_2/CNTs were characterized. They showed good hydrophilicity (contact angle: 85.9°), high specific surface area (96.68 m^2/g) and high specific capacitance (87.6 F/g). The experimental results illustrated that the best DE was achieved by the composites (60%T/C) under 1.2 V with the maximum electrosorption capacity toward 6.5 mg/g, and the TiO_2/CNTs composites had excellent stability. Adsorption kinetics analysis was explored and analyzed. Furthermore, TiO_2/CNTs composites exhibited excellent DE in actual desulfurization wastewater. The catalysis and adsorption mechanisms of the TiO_2/CNTs anode were discussed in detail. This study provides a new direction for the application of TiO_2/CNTs composites as adsorption materials of CDI in the Cl^- of desulfurization wastewater.

Key words: capacitive deionization, dechlorination performance, desulfurization wastewater, TiO_2/CNTs composites

HIGHLIGHTS

- The TiO_2/CNTs materials were used as adsorption materials for a CDI anode to remove Cl^- from desulfurization wastewater.
- TiO_2/CNTs were synthesized by using a solvothermal method based on Ti^{4+} combining NMP along with CNTs as precursor solution.
- This study will provide a new direction for the application of TiO_2/CNTs composite material as adsorption materials for CDI in actual desulfurization wastewater.

GRAPHICAL ABSTRACT

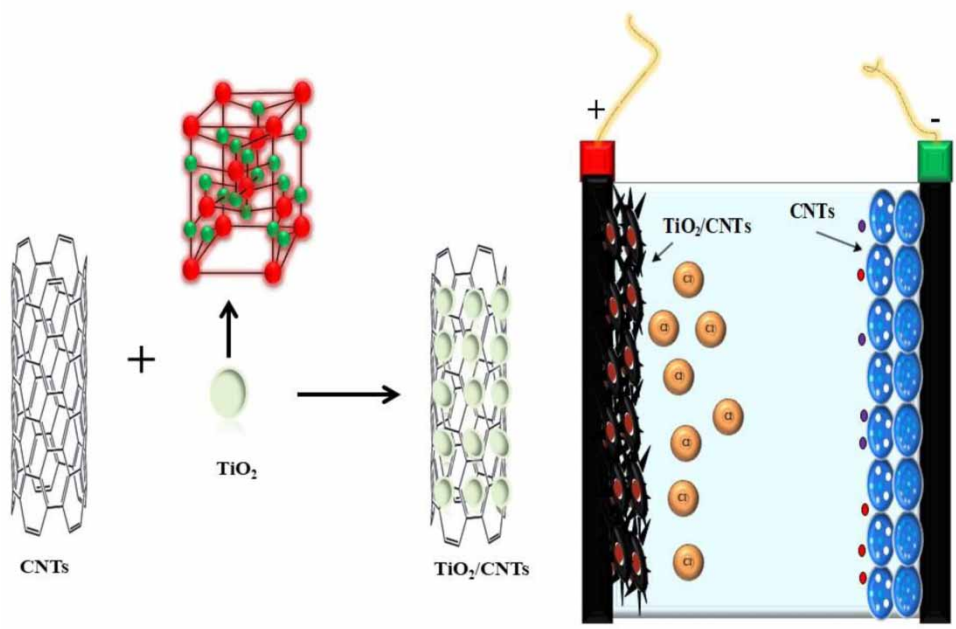

1. INTRODUCTION

Desulfurization wastewater mainly contains high levels of supersaturated nitrite, sulfite, suspended solids, heavy metal ions, F^- and Cl^-, etc. (Shuangchen *et al.* 2016). It is worth noting that the increase in Cl^- concentration in desulfurization wastewater will bring many problems (Zheng *et al.* 2019). On the one hand, it will lead to a decline in the quality of gypsum. On the other hand, the increase in Cl^- content will increase the acidity of wastewater and affect desulfurization efficiency. In addition, the corrosion of system materials will be intensified with an increased concentration of Cl^-. Therefore, the main goal of current wastewater treatment technology is to improve dechlorination efficiency.

The traditional treatment method (Gingerich *et al.* 2018b; Ma *et al.* 2019) mainly adopts the chemical dosing method to remove a large number of calcium ions, magnesium ions and some heavy metal ions from wastewater, such as the common triplet-tank treatment technology, double alkali method, etc. There are two main methods of wastewater concentration and reduction: membrane methods and thermal methods. For example, the widely used reverse osmosis (RO) (Conidi *et al.* 2018), forward osmosis (FO) (Lee *et al.* 2018b), nanofiltration (NF) (Jia & Wang 2018), electrodialysis (ED) (Luo *et al.* 2019) and so on have been applied. Thermal concentration technology mainly uses steam for evaporation and crystallization of wastewater, including mechanical vapor recompression (MVR) (Gingerich *et al.* 2018a), thermal vapor recompression (TVR) (Hassan & Darwish 2014), multi-effect evaporation (MED) (Iaquaniello *et al.* 2014) and evaporation are in use with waste heat of power plant flue gas. Although much research has been carried out on the treatment of desulfurized wastewater, traditional water treatment technology still faces the problems of large modification of the original system and high investment cost. Based on comprehensive analysis, there is an urgent need to find a new technology for removing Cl^- from desulfurization wastewater as key to solving the problem.

As a new wastewater treatment technology in recent years, capacitance deionization technology (CDI) (Porada *et al.* 2013; Suss *et al.* 2015; Jia & Zhang 2016) has attracted wide attention from scholars due to its advantages of low energy consumption, convenient operation, simple maintenance and good removal efficiency. CDI technology has been studied in seawater (Jande & Kim 2014; García-Quismondo *et al.* 2016), brackish water (Tang *et al.* 2016; Xing *et al.* 2019), circulating cooling wastewater (Ma *et al.* 2018), printing and dyeing wastewater (Senoussi & Bouhidel 2018) and other fields. Unlike RO, CDI does not require high pressure or temperature, and it can be operated at room temperature with low voltage. Compared with ED, CDI does not use ion exchange membranes, so it does not cause membrane clogging or require high feed water quality. Indeed, the flue gas concentration tower is more acidic and it very easy to cause corrosion in the equipment. In contrast,

CDI is a good way to avoid such occurrences because it does not require dosage and generate secondary contamination. In addition, there is not enough space to build a desulfurization wastewater treatment device at the end of the power plant, and the small footprint of CDI is an effective solution to this problem. Therefore, the use of CDI as a reduction unit for desulfurization wastewater has great advantages and broad application prospects.

The CDI principle is to form an electrical double-layer (EDL) (Jia & Zhang 2016) on the surface of the electrode through the action of electric field force to collect charged ions in water by using the electrochemical characteristics of the surface of the charged electrode. Among them, adsorption materials have always been the research focus of this technology as an important factor of CDI. Carbon materials (Huang *et al.* 2017) are commonly used for adsorption materials. The general carbon materials include activated carbon (Kim *et al.* 2016; Hu *et al.* 2018), graphene (Shi *et al.* 2016), activated carbon fiber (Tian *et al.* 2019), carbon aerogel (Quan *et al.* 2017; Liu *et al.* 2019) and carbon nanotubes (Lee *et al.* 2018a). Carbon nanotubes (CNTs) have been widely studied and discussed, because of their large specific surface area and good electrical conductivity. Therefore, how to improve the electrical adsorption efficiency of CNTs is key to the research. Surface treatment or loading of other materials can effectively improve adsorption efficiency. Metal oxides on carbon-based substrates can enhance conductivity, improve specific capacitance (Zhang *et al.* 2009) and increase charge storage (Boukhalfa *et al.* 2012). Furthermore, the addition of metal oxides can significantly change the physical and chemical properties of some carbon materials, such as wettability, surface area and zeta potential, which is helpful to improve the deionization performance of capacitors. TiO_2 is a kind of n-type oxide, environment-friendly semiconductor material with high stability, high-quality hydrophilicity, and low cost. The wettability and electrochemical performance of carbon materials can be effectively increased by TiO_2-loaded carbon materials to improve electric adsorption efficiency (Cheng *et al.* 2019). Therefore, the combination of TiO_2 semiconductor materials and CNTs porous materials as composite adsorption materials can effectively improve the adsorption efficiency of CDI.

Solvothermal methods have been commonly used to coat TiO_2 onto the surface of CNTs (Liu *et al.* 2013). Muduli *et al.* (2009) synthesized TiO_2-multiwalled carbon nanotube (MWCNT) nanocomposites using a hydrothermal method, the results showed the TiO_2-MWCNT conjugation through -COOH groups, and that it had efficient charge transfer in the nanocomposites. Yi *et al.* (2016) reported that TiO_2@CNTs materials had been successfully achieved by a polymer-assisted approach to an aqueous chemical solution method. The polymer, polyethylenimine, aims to combine the Ti^{4+} with CNTs for film formation of TiO_2@CNTs. This approach can prevent ion hydrolysis in solution and form a conformal coating for complex structure. Noteworthily, N-methyl pyrrolidone (NMP) is a good polymer solvent (Kim *et al.* 2006; Sotto *et al.* 2011). Inspired by these, to explore a simple, low-cost, and energy-efficient synthetic strategy, a novel preparation method of TiO_2/CNTs was developed in this study. This research has prepared Ti^{4+} combining NMP along with CNTs and forming a stable and homogeneous precursor solution to fabricate TiO_2/CNTs.

In this study, TiO_2/CNTs were synthesized using a solvothermal method based on Ti^{4+} combined with NMP along with CNTs as precursor solution. Materials were used for the first time as adsorption materials for CDI anode to remove Cl^- from desulfurization wastewater. Physical characteristics of composites were discussed, and cyclic voltammetry (CV) was used to analyze the electrochemical performance of the composites. Finally, TiO_2/CNTs composites was modified on the surface of the CDI anode to experiment with Cl^- removal to find the best composites. The electrosorption method was analyzed and discussed by the adsorption kinetic model and the adsorption mechanism of TiO_2/CNTs was also explored. This study will provide a new direction for the application of TiO_2/CNTs composites as adsorption materials of CDI in the actual desulfurization wastewater.

2. EXPERIMENTAL METHOD

2.1. Preparation of adsorption material

The process of material preparation is shown in Figure 1. Here, 0.5 g multi-wall carbon nanotubes (MWCNTs, xfm01, Aladdin, Shanghai) were dissolved in 20 mL NMP and used as the polymer solvent (Ma *et al.* 2019), 40 mL absolute ethanol was added, and then the mixture was fully stirred on a magnetic stirrer (Qiuzo DF-101S, Zhengzhou). In the process of stirring, 2 mL tetrabutyl titanate were added dropwise and used as a precursor of TiO_2 nanoparticles. After stirring for 30 min, the mixed solution was transferred to the polytetrafluoroethylene reactor, and removed after leaving it in the oven at 200 °C for 12 h. After the reaction, the reactor was naturally cooled to room temperature, the precipitates were collected, centrifuged, and washed with water and ethanol three times, dried in a blast drying oven at 60 °C for 12 h, and the resulting solid powder

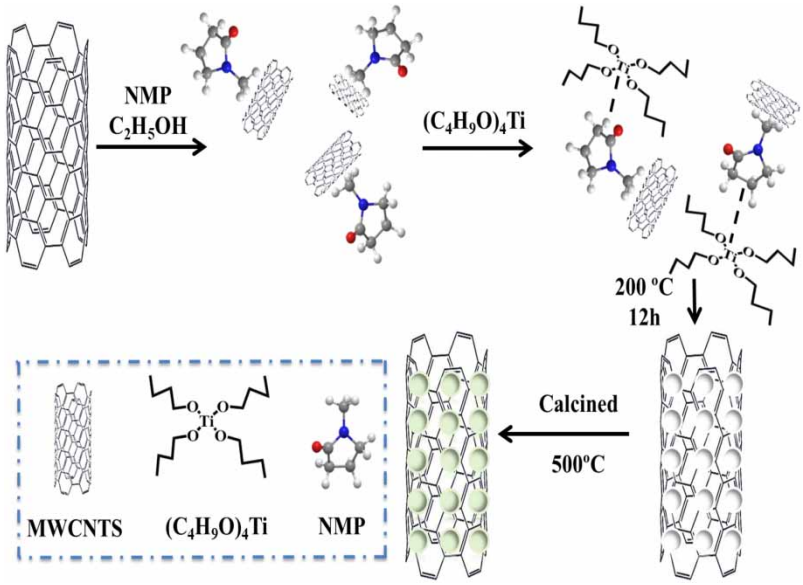

Figure 1 | Synthetic schematic of TiO_2/CNTs composites.

was placed in a muffle furnace and sintered at 500 °C. The final product was the TiO_2/CNTs composite. The composites prepared at this ratio were recorded as 60%T/C (the content of TiO_2 accounts for 60% of the total sample). According to this method, composites with different proportions were prepared, and recorded as 15%T/C and 30%T/C. The chemicals and reagents used were purchased from the Tianjin Beichen Founder Reagent Factory for analytical purity in the experiment.

2.2. CDI electrode material

The anode electrode plates of CDI were prepared by weighing 0.2 g of composites at different ratios, mixing with acetylene black and polyvinylidene fluoride at a ratio of 8:1:1 and dissolving them in an appropriate amount of NMP. The mixed solution was sonicated for 15 minutes with an ultrasonic cleaner (020S, Shenzhen Genen Cleaning Equipment Co. LTD), followed by centrifugation at 5,000 rpm for 10 min and magnetic stirring. The stirred dispersion was added evenly to the 10 cm × 10 cm titanium plate using a rubber-tipped dropper, followed by smoothing the raised portion using a glass rod and drying for 12 hours at room temperature. All experiments were carried out at 25 °C. Similarly, multiwalled CNTs modified CDI cathode electrode plates were prepared.

2.3. Characterization method

X-ray powder diffraction (XRD) analysis was performed using an X-ray diffractometer (D8advance, Buker, Germany). CuKα ($\lambda = 0.6491$ nm) was used, for which the tube voltage was 40 kV, the tube current was 40 mA, the scan step width was 0.026°, the counting time was 10 s, and the scan angle was 2θ from 5 to 80°. A scanning electron microscope (SEM) (S-4800, Hitachi, Japan) was used to observe the morphology of the adsorbed material. The sample was weighed and dispersed in anhydrous ethanol, and the homogeneous dispersion was prepared by sonication. A small amount of the dispersion was removed and added dropwise on a smooth single crystal wafer substrate and dried naturally. The composites were observed using a transmission electron microscope (TEM) (Jem-2100F, Jeol, Japan). An X-ray photoelectron spectroscopy (XPS) model (250xi, Therom Escalab, USA) with Al target, 100 μm beam spot and 25 W power parameters was used to further analyze the elemental content of the composites surface after the adsorption experiment. The surface groups of the TiO_2/CNTs composites were studied by Fourier transform infrared spectroscopy (FT-IR) using an instrument model (Spectrum 100, Perkin Elmer, Inc., USA). The wettability in terms of static water contact angle (WCA) of materials was tested using an OCA15EC (Dataphysics, Germany) instrument. The specific surface area, pore size distribution, and pore size were measured using the Brunauer–Emmett–Teller (BET) method on the basis of N_2 adsorption–desorption isothermal at 77.35 K using the Auto-sorb-iQA3200-4 (Quantatech Co., USA) instrument.

2.4. Electrochemical performance test

All electrochemical tests used the CHI760E electrochemical workstation, employing a three-electrode system: a Glassy Carbon Electrode (GCE) as the working electrode (WE), Pt as the counter electrode (CE), and a Saturated Calomel Electrode (SCE) as the reference electrode. The electrolyte was 1 M NaCl solution, which needed to be replaced before each test. Preparation of the working electrode was as follows: weighed 40 mg of sample powder and put it into a centrifuge tube containing 2 mL of anhydrous ethanol. After ultrasonic cleaning for 30 min, 40 μL of Nafion solution was added and ultrasound treatment was continued until it was evenly dispersed. We transferred 120 μL of the obtained dispersion to evenly coat the conductive surface with an area of 1 cm × 2 cm. This was repeated three times for a total of 360 μL. The specific capacitance of activated carbon was estimated by CV curve. In the voltage range of 0–0.8 V, the scanning rates were 1 mV/s, 5 mV/s, 10 mV/s, 50 mV/s and 100 mV/s, respectively. The specific capacitance value could be determined by the following formula (Gan *et al.* 2019):

$$C = \frac{\int_{Va}^{Vc} I\, dV}{2mv(Vc - Va)} \tag{1}$$

where C represents specific capacitance, F/g; Vc and Va represent the highest and lowest voltage of CV test, V; I represents current density, A/m^2; V represents scanning rate, mV/s; and m represents the mass of the active material, g.

2.5. CDI device construction

The capacitance deionization experimental device and system flow chart used in the experiment of CDI device are shown in Figure 2(a) and 2(b) respectively. The device adopted the traditional CDI structure. There were two fixed end plates on the outside, and the negative and positive electrode plates were close to the endplate. A filter was sandwiched in the middle of the two electrode plates to provide a reaction area for the solution to be treated; the outer side was sealed with a rubber pad. The solution entered from the bottom left of the figure and passed through the middle of the two electrode plates from the bottom to the top. The purpose was to allow the solution to be fully adsorbed.

2.6. Desalination performance test

This experiment adopted the batch mode method to deal with 200 mL NaCl solution. Before the test, the equipment should be fully cleaned with deionized water. The change in Cl^- concentration was monitored by a potential ion meter (PXSJ-216F), and the real-time data were recorded every 15 seconds until the Cl^- concentration tended to be stable over a certain range.

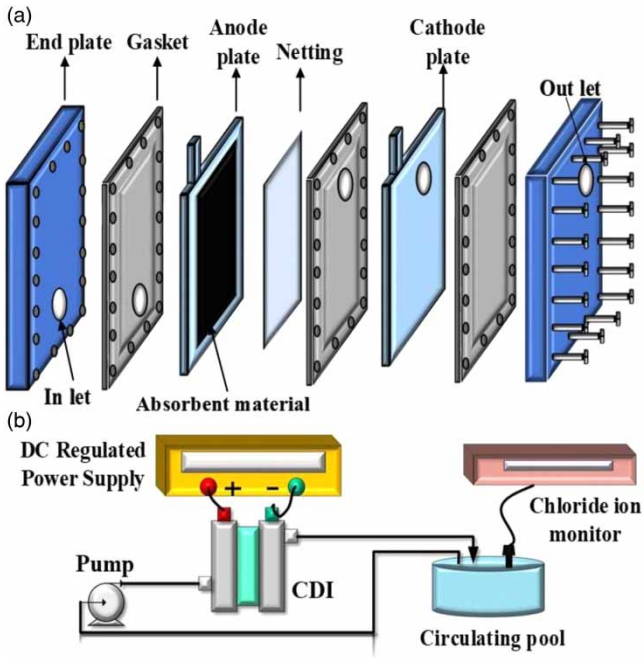

Figure 2 | (a) CDI device structure; (b) CDI dechlorination flow chart.

This experiment was divided into three parts to analyze the DE of the CDI device, which were the different ratios of composites, different voltages and different initial concentrations. In addition, the desalination performance of the material was also analyzed in this experiment. The conductivity could be transformed into concentration through the calibration test experiment by monitoring and measuring the conductivity with a conductivity meter. The electrosorption capacity (EC, mg/g), the amounts of adsorbed ions per gram of membrane electrode, could be calculated by the following Equation (2):

$$EC = \frac{(C_0 - C_E)V}{m} \tag{2}$$

where C_0 and C_e represent the NaCl solution of initial concentration and equilibrium concentration (mg/L), V (L) is the volume of NaCl aqueous solution, and m (g) is the total mass of electrode material.

3. RESULTS AND DISCUSSION

3.1. Characterization analysis

3.1.1. XRD

Figure 3(a) shows the XRD spectra of CNTs and TiO_2/CNTs composites. There are obvious diffraction peaks at 26.2°, corresponding to the (002) crystal surface of CNTs (Yi *et al.* 2016), which indicates that CNTs exist in TiO_2/CNTs composites. In

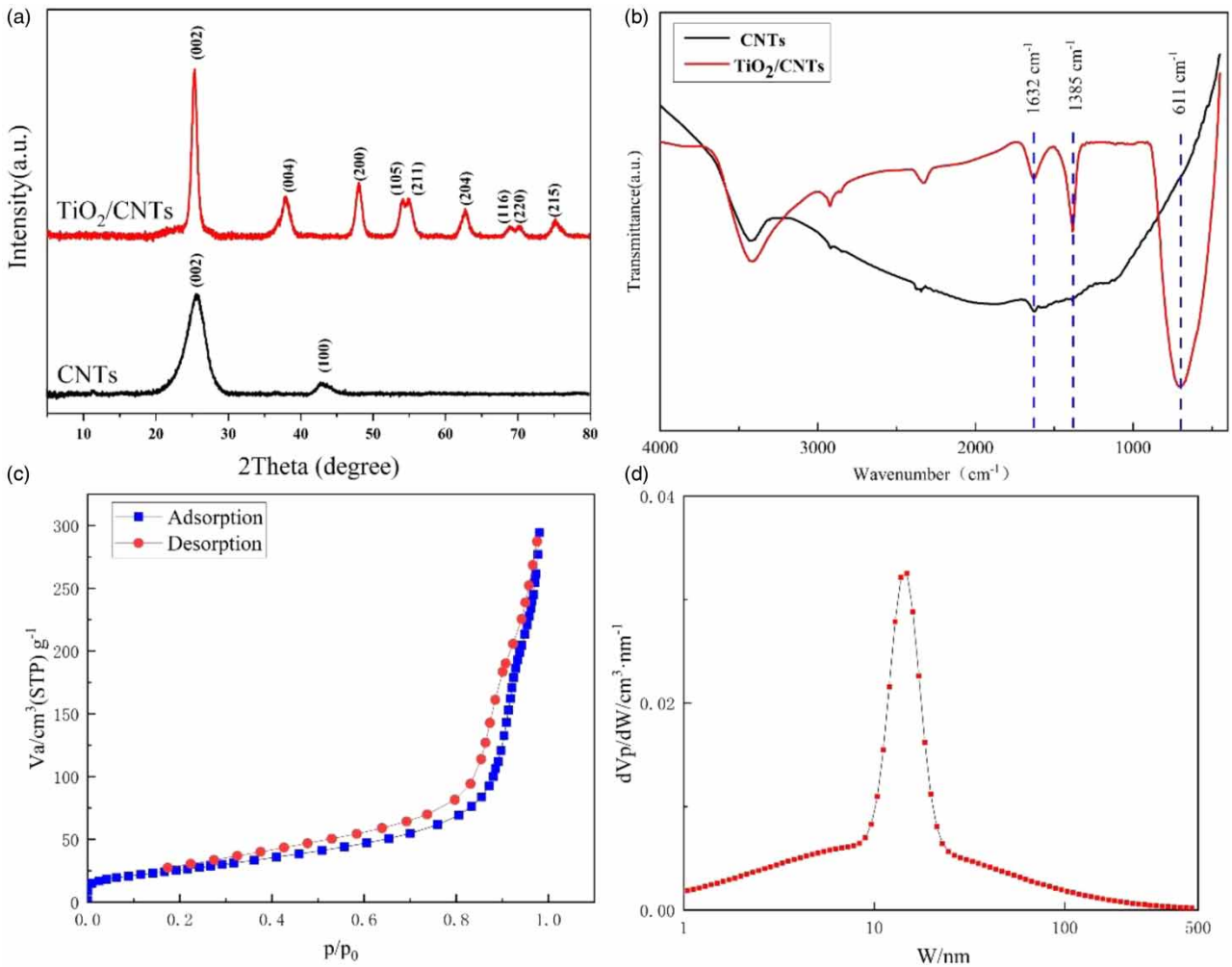

Figure 3 | (a) XRD spectrum of CNT_S and TiO_2/ CNTs; (b) FT-IR spectrum of CNTs and TiO_2/CNTs composites; (c) N_2 adsorption–desorption isotherms; (d) pore size distribution curve.

the spectrum of TiO_2/CNTs composites, the diffraction peaks of 25.356°, 37.785°, 48.076°, 53.920°, 55.114°, 62.726°, 70.357° and 75.094° are located at (101), (004), (200), (105), (211), (204), (215) of TiO_2 respectively, corresponding to the characteristic peaks of TiO_2 (JCPDS No. 37-1492) (Wang *et al.* 2013). This indicated that our samples contained both anatase TiO_2 phase and CNTs as expected. There was no other obvious characteristic peak, which showed that the composites had high purity and good crystal phase.

3.1.2. FT-IR

To further study the surface groups of TiO_2/CNTs composites, Fourier transform infrared spectroscopy (FT-IR) was used to analyze the composites to verify the successful construction of molecular imprinting sites of the composites (Liu *et al.* 2017). In Figure 3(b), there are vibration bands at 1,632 cm^{-1} and 1,385 cm^{-1}; the bands at 1,632 cm^{-1} are related to the C=C bond, while the bands at 1,385 cm^{-1} are related to the C–C bond. However, at 611 cm^{-1} the TiO_2/CNTs composites had a large wave band, while CNTs material did not. This is related to the Ti-O structure and O-Ti-O structure in TiO_2 (Nguyen *et al.* 2016). It can be seen that TiO_2/CNTs composites have the chemical bond characteristics of CNTs and TiO_2 materials.

3.1.3. BET and SEM

In order to investigate the pore structure of the TiO_2/CNTs materials, the N_2 adsorption–desorption isotherms are acquired. The tests results are listed in the Table 1 and Figure 3(c). The adsorption–desorption isotherm exhibits the typical feature of a type IV isotherm, indicating the presence of many mesopores inside both samples, this result was also indicated by the pore size distribution curve in Figure 3(d).

Figure 4(a) shows SEM images of CNTs. It can be seen that the CNTs are distributed in disorderly spun filaments. Figure 4(b) shows SEM images of TiO_2/CNTs composites. Compared with a single CNTs, the surface of the TiO_2/CNTs composites is a cluster of coral, the surface is rough and densely distributed. It is easy for ions to adhere to the material and provide more adsorption sites, which indicates that the TiO_2/CNTs composites had high efficiency of electrosorption (Zhu *et al.* 2015). Due to the high content of powdered TiO_2 which wraps the CNTs material, the shape of spinning is not obvious in the figure.

3.1.4. TEM

Figure 4(c) is the TEM diagram of TiO_2/CNTs composites which is the full picture of the composites. It can be seen that there are many TiO_2 nanoparticles attached to CNTs. The staggered lattice stripes indicate the formation of heterojunctions between TiO_2 and CNTs. Figure 4(d) is the high-resolution transmission electron microscope (HR-TEM) image which shows that the nanohybrids TiO_2/CNTs are highly crystalized. The uniform lattice fringes of TiO_2 nanoparticles show that they are highly crystallized, and d is 0.3520 nm corresponding to the (101) crystal surface of anatase TiO_2 (Olowoyo *et al.* 2019), which is consistent with the XRD results. The above results show that the TiO_2/CNTs composites were successfully prepared.

3.1.5. XPS

To determine the chemical composition and valence state of elements in the TiO_2/CNTs composites, the elements Ti, O and C in 60%T/C composites were analyzed by XPS. Figure 5(a) shows the full spectrum of the sample. Figure 5(b) shows the high-resolution XPS spectrum of Ti2p. The binding energies at 458.47 eV and 464.1 eV correspond to $Ti2p_{3/2}$ and $Ti2p_{1/2}$ of Ti^{4+} (Olowoyo *et al.* 2019). Figure 5(c) shows that the characteristic peaks of the O1s spectrum are at 529.6 eV, which is attributed to Ti-O lattice oxygen (Hafeez *et al.* 2018). Figure 5(d) shows that the characteristic peak of C1s is located at 284.82 eV, which is attributed to the C–C bond and C=C bond in CNTs (Cong *et al.* 2011). Table 2 is the composition analysis table of TiO_2/CNTs composites. The peak intensities of Ti2p and O1s were 22031.39 cps and 8066.21 cps, respectively, which were much higher than those of C1s (7282.05 cps). By calculating the atomic ratio, Ti2p:O1s:C1s is 4:2:4. XPS results further prove that the formation of heterojunction between TiO_2 and CNTs is consistent with TEM results.

Table 1 | Surface area properties of TiO_2/CNTs

	S_{BET} (m^2/g)	V_{meso} (cm^3/g)	Mean pore diameter (nm)	Average pore diameter (nm)
Value	96.68	22.213	18.842	0.4554

Where S_{BET} represents specific surface area, V_{meso} represents pore volume.

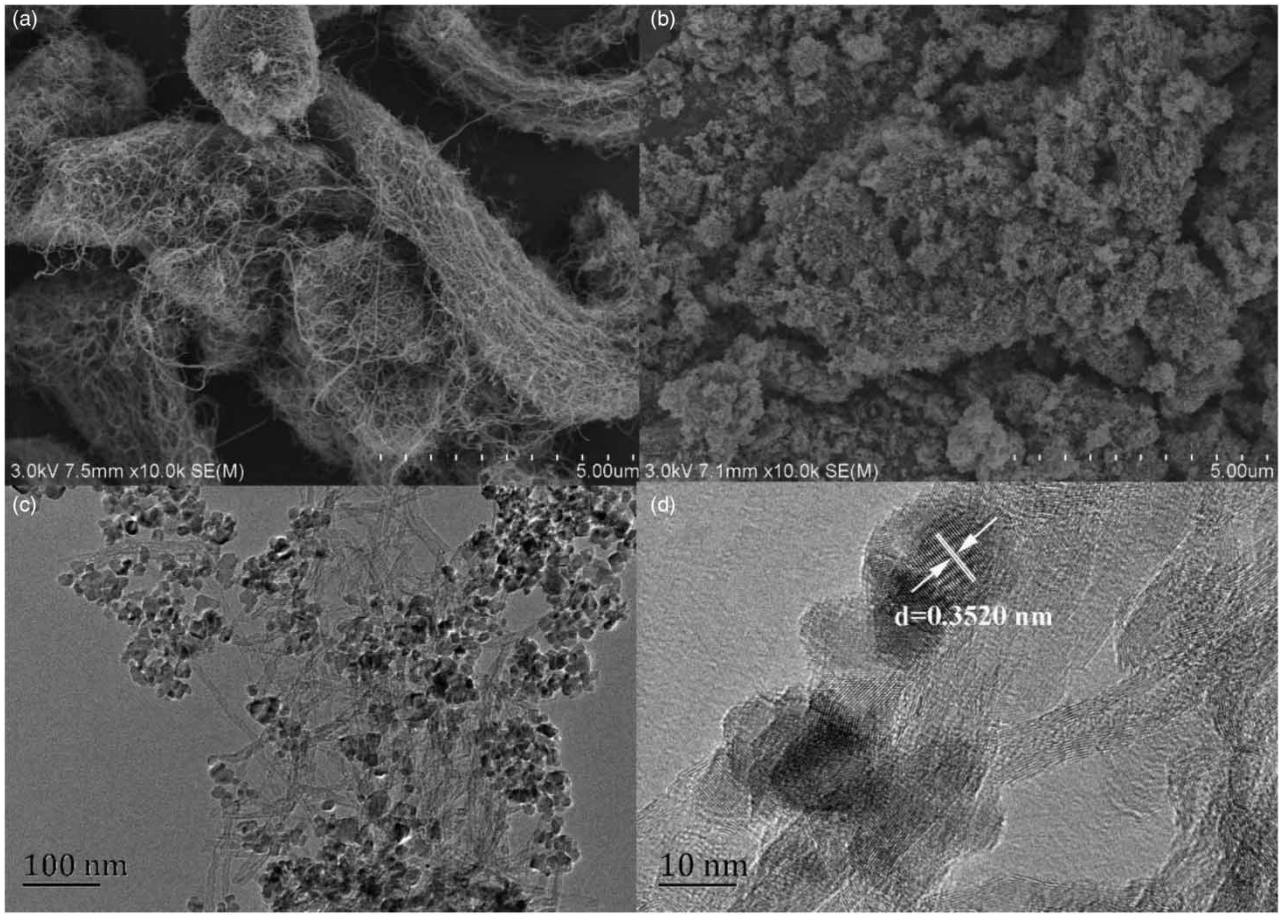

Figure 4 | (a) SEM images of CNTs; (b) SEM diagram of TiO_2/CNTs composites; (c) TEM and (d) HR-TEM diagram of TiO_2/CNTs composites.

3.1.6. Wettability

The wettability of the CDI adsorbent material is critical. The WCA of CNTs and TiO_2/CNTs composites was determined, and the findings are shown in Figure 6(a) and 6(b). It can be seen that the WCAs of CNTs and TiO_2/CNTs composites are 124.6° and 85.9°, respectively. The results demonstrate that the addition of TiO_2 significantly enhanced the wettability of the CDI adsorbent material (Zheng *et al.* 2018). which could have a positive impact on improving adsorption performance of CDI.

3.2. Electrochemical performance test

Specific capacitance is an important index to test the electrosorption properties of materials (Nguyen *et al.* 2016). Figure 7(a) shows the cyclic voltammetric test results of different adsorbed materials in the range of 0–0.8 V at a sweep rate of 100 mV/s. It can be seen from the observation diagram that the images are all in rectangular distribution, which shows that there was no redox reaction in the scanning process. But the EDL capacitance plays a leading role, and the adsorption of ions was due to the interaction between the Coulomb forces rather than the electrochemical reaction (Quan *et al.* 2017). In addition, the larger is the surrounding area, the larger is the capacitance of the material. Therefore, it is easy to see that the capacitance of the adsorption materials is larger than pure CNTs, and the composites with 30%T/C and 60%T/C ratio had a larger capacitance. Figure 7(b) shows the cyclic voltammogram of the 60%T/C material at 1 mV/s, 5 mV/s, 10 mV/s, 50 mV/s and 100 mV/s scanning speed. According to Equation (1), the specific capacitance of each sweep speed was 87.6 F/g, 42.6 F/g, 32.8 F/g, 2.1 F/g and 1.7 F/g. The observed data show that the specific capacitance was inversely proportional to the scanning rate. This is because, at a higher scanning rate, sodium ions and chloride ions do not have enough time to accumulate and enter the internal holes of the electrode, and the ohmic resistance will increase correspondingly, resulting in a lower specific capacitance (Feng *et al.* 2019).

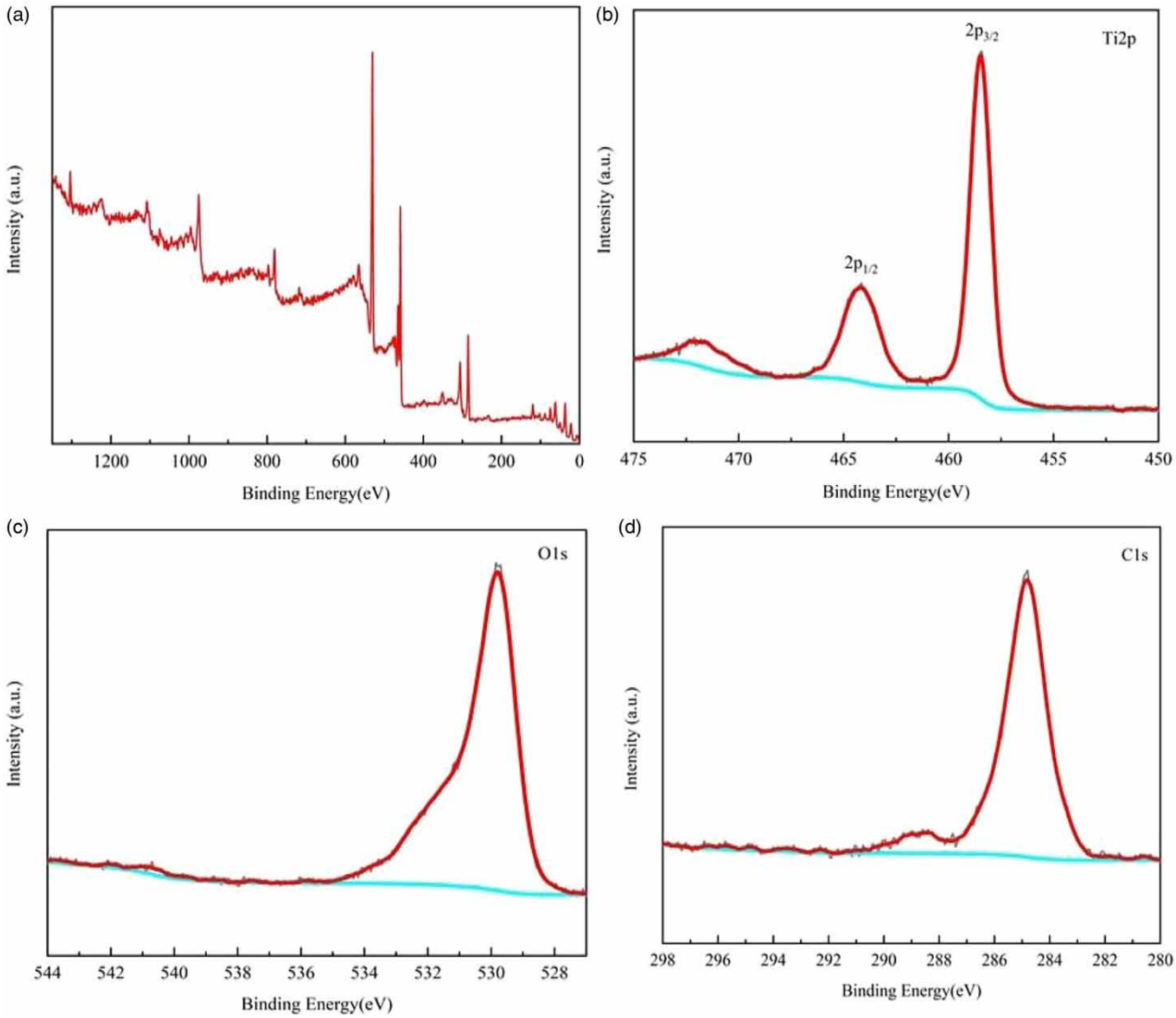

Figure 5 | (a) XPS diagram of TiO_2/CNTs composites; (b) XPS diagram of Ti2p; (c) XPS diagram of O1s; (d) XPS diagram of C1s.

Table 2 | Composition analysis table of TiO_2/CNTs composites

Name	Start BE	Peak BE	End BE	Height CPS	FWHM eV	Area (P) CPS.eV	PP At. %
C1s	299	285	280	7282	1.65	15838	41
Ti2p	476	458	449	22031	1.15	48667	20
O1s	546	529	526	28066	1.59	62155	39

3.3. DE of materials

Voltage is an important index affecting the performance of CDI. Select the adsorption materials with a 60%T/C ratio to carry out dechlorination experiments under the voltages of 0.4 V, 0.8 V, 1.2 V and 1.5 V under flow rate of 50 mL/min. The data are shown in Figure 8(a). It is expected that the higher the voltage, the better the DE. This is because when the voltage increases, the amount of charge carried on the plate increases (i.e. the electric field force increases), and more chloride ions can be

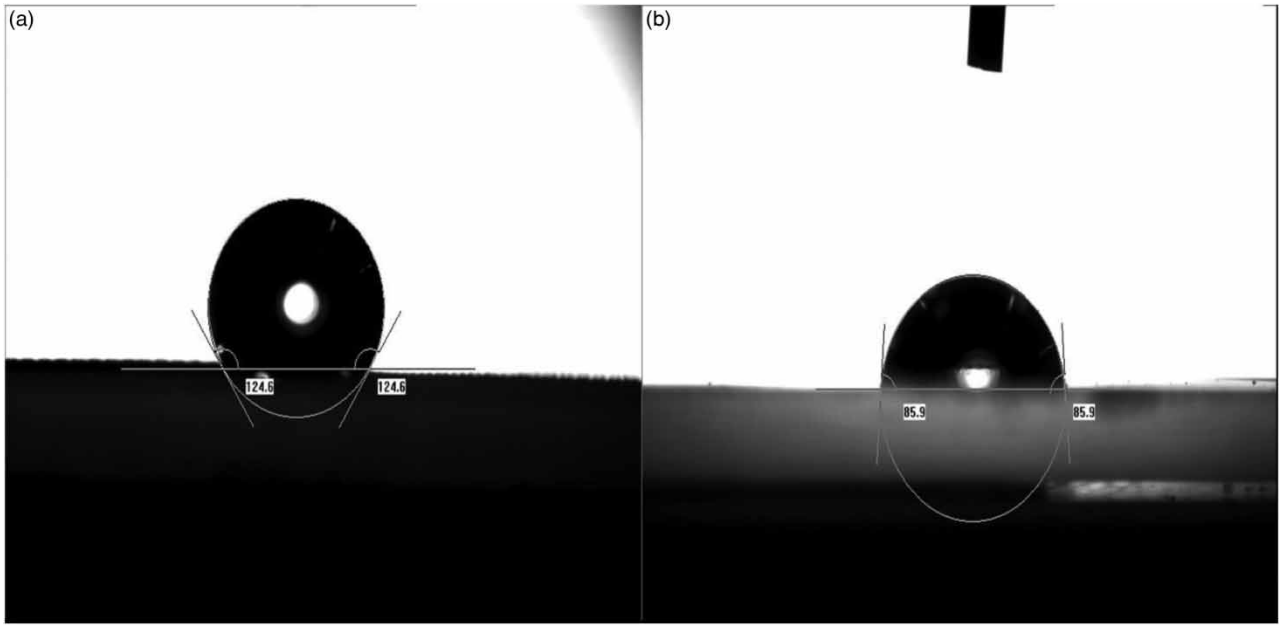

Figure 6 | (a) Water contact angle of CNTs; (b) water contact angle of TiO_2/CNTs.

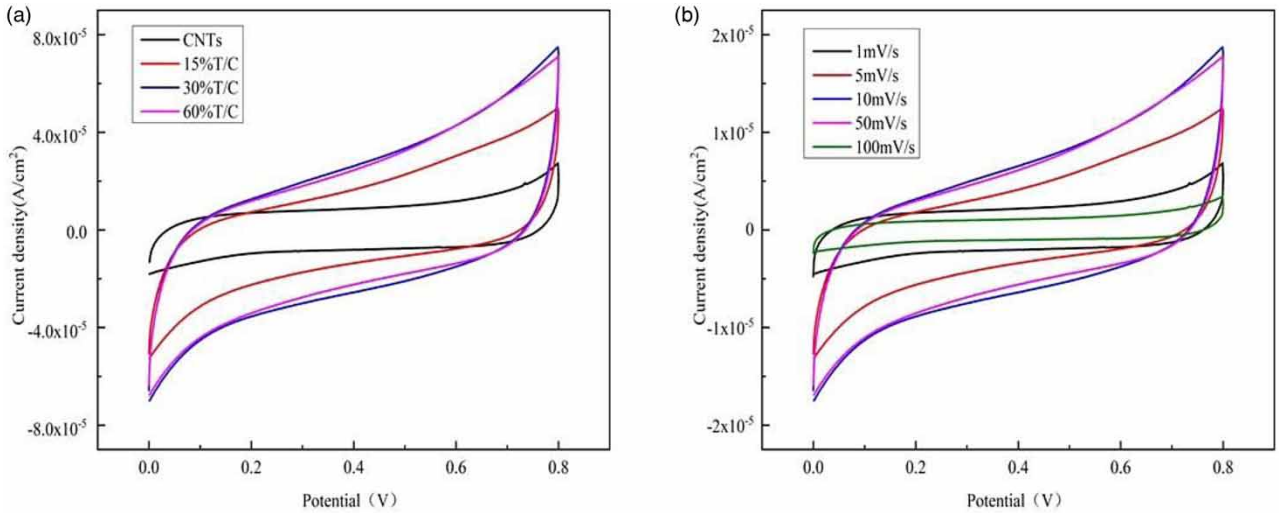

Figure 7 | (a) Cyclic voltammetric (CV) curves of different adsorption materials; (b) CV curves of 60%T/C materials at different scanning speeds.

adsorbed in unit time. It can be found in the observation chart that the trend is consistent with the voltages of 0.4 V, 0.8 V and 1.2 V. However, compared with conditions of 1.2 V and 1.5 V, the DE of 1.2 V is better than 1.5 V. This may be due to the hydrolysis reaction (Reddy & Reddy 2006) that occurs when the voltage is about 1.23 V, resulting in a large amount of OH^- in the solution; the charge used to adsorb ions will lose part of it to participate in the hydrolysis reaction. Furthermore, OH^- and Cl^- have a competitive relationship, which will inhibit Cl^- adsorption on the electrode surface. To sum up, it is not difficult to see that the composites have the best DE under the voltage of 1.2 V.

To compare the DE of different adsorption materials, under the condition of 1.2 V voltage, 100 mg/L initial concentration and 50 mL/min flow rate, a 200 mL NaCl solution was treated by batch mode. The results are shown in Figure 8(b). It can be seen that with the increase in the TiO_2 ratio, the DE is improved. To sum up, it can be concluded that the optimal composites ratio is 60%T/C. This may be because TiO_2 loading on CNTs can effectively improve the hydrophilicity of the material, and

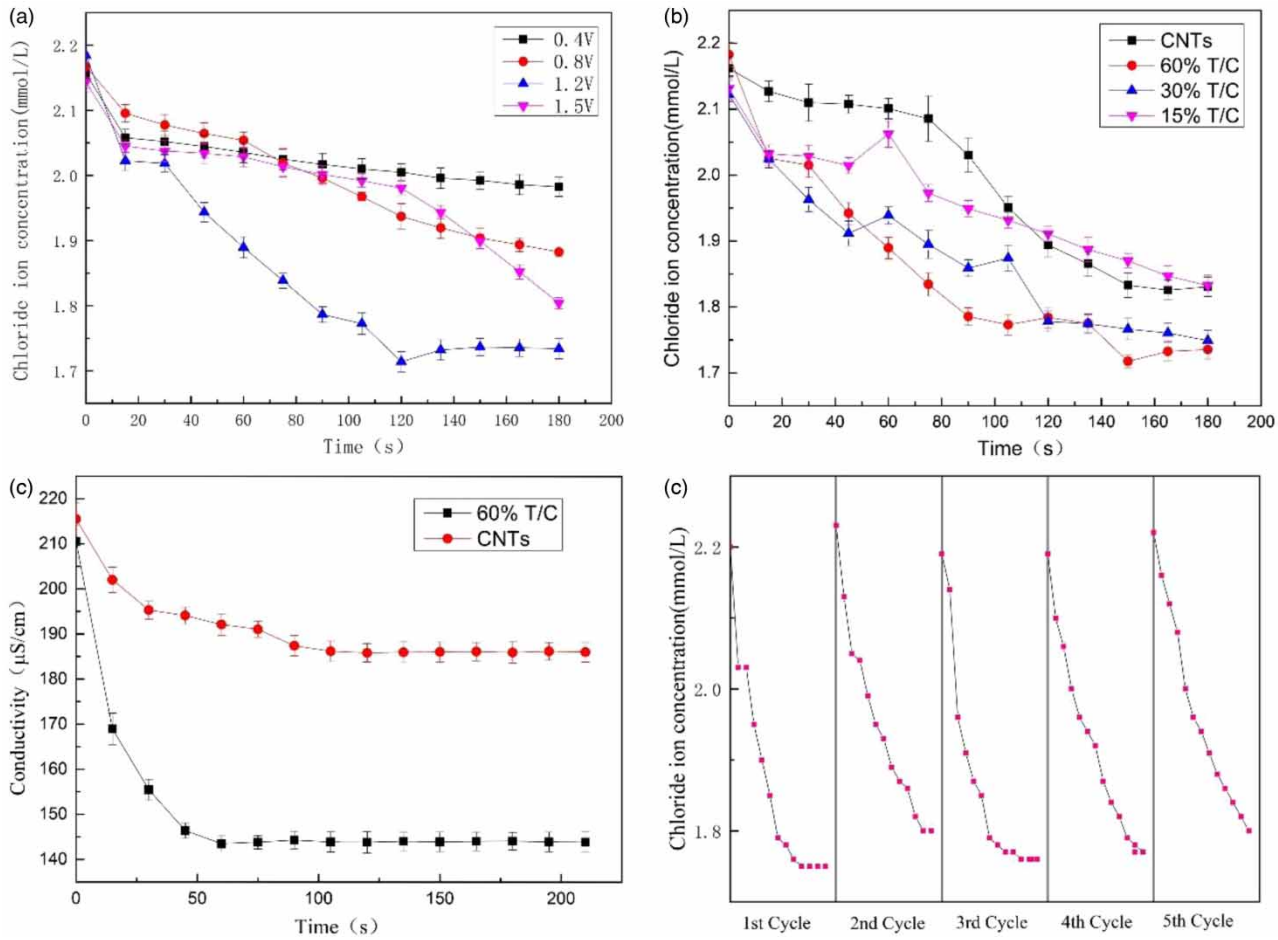

Figure 8 | (a) 60%T/C DE under different voltage; (b) DE of different materials used in CDI device; (c) desalination curve of different materials; (d) cyclic experiment of 60%T/C electrode.

TiO_2 as an excellent semiconductor material can improve the efficiency of catalytic. Furthermore, the increase in titanium atoms can provide more adsorption sites for the adsorption of Cl^- (Li *et al.* 2016).

To compare the adsorption performance of TiO_2/CNTs composites and CNTs material, the desalination capacity of 60%T/C composites and pure CNTs was analyzed. Both experiments were carried out under the conditions of an initial concentration of 100 mg/L NaCl, a flow rate of 50 mL/min and a voltage of 1.2 V. The desalination performance efficiency is shown in Figure 8(c). The conductivity curves of the two materials show a downward trend and tend to be stable after a certain period. However, the decline of 60%T/C composites was much larger than that of pure CNTs. According to Equation (2), the EC of 60%T/C composites and pure CNTs was 6.5 mg/g and 3 mg/g respectively. Furthermore, according to the previous reports of TiO_2/CNTs composites used for CDI (Table 3), it can be seen that the adsorption material shows good electrosorption performance.

The long-term stability of the system is an important indicator to test the performance of the adsorbent material. Figure 8(d) shows the ion adsorption of five cycles of the 60%T/C electrode with an initial concentration of 100 mg/L NaCl under a voltage of 1.2 V and a flow rate of 50 mL/min. Observing the downward linear trend, it can be found that the DE performance of TiO_2/CNTs did not change significantly, which manifests outstanding cycle to cycle durability.

3.4. The kinetic analysis

The adsorption capacity of Cl^- by 60%T/C composites at different initial concentrations was studied by using pseudo first-order and pseudo second-order kinetic models. The pseudo first-order and pseudo second-order dynamic models are

Table 3 | Research results of TiO_2/CNTs composites for CDI

Electrode	Initial concentration	Voltage (V)	Electrosorption capacity (mg/g)	Reference
TiO_2/CNTs	500 (mg/L)	1.2	~4.3	Reddy & Reddy (2006)
Graphene/CNTs	57 (μs/cm)	2.0	1.41	Zhang *et al.* (2012)
Graphene oxide	150 (μs/cm)	1.2	1.31	Moustafa *et al.* (2020)
Activated carbon	100 (mg/L)	1.2	~5.43	Liu *et al.* (2013)
60%T/C	100 (mg/L)	1.2	6.5	This paper

calculated according to Equations (3) and (4) (Gaikwad *et al.* 2020), respectively, as follows:

$$\log(q_e - q_t) = \log q_e - \frac{k_1}{2.303}t \tag{3}$$

$$\frac{t}{q_t} = \frac{1}{k_2 q_e^2} + \frac{t}{q_e} \tag{4}$$

Among them, t is the electrosorption time, k_1 is pseudo-first order model constants and k_2 is pseudo-second order model constants, while C_0, C_t and C_e represent the initial concentration, the concentration at t time and the concentration at equilibrium, respectively.

Table 3 shows the reaction rate constant K-value and correlation coefficient R^2 of the pseudo first-order and the pseudo second-order kinetic models at different initial concentrations. It can be seen from the comparison of R^2 that the fitting degree of a pseudo first-order dynamic model to 60%T/C composites was higher. Figure 9(a) is a linear diagram of the adsorption kinetics of 60%T/C composites fitted by a pseudo first-order kinetic model. Combining Table 4 and Figure 9(a), it can be seen that the higher the concentration, the better the adsorption capacity.

The CDI Ragone plot as a functional tool to evaluate desalination performance in CDI, it is more applicable when considering the electrosorption behavior of a material (Kim & Yoon 2015). To this end, the initial salt concentration affecting the DE was examined. As shown in Figure 9(b). Higher salt concentrations shift the curve to the upper right. This means that both the deionizing capacity and the average deionizing rate have increased, which is similar to the conclusion of the kinetic model. The increase in capacity is primarily due to the compaction of the double layer and the subsequent rise in capacitance (Kim & Yoon 2013).

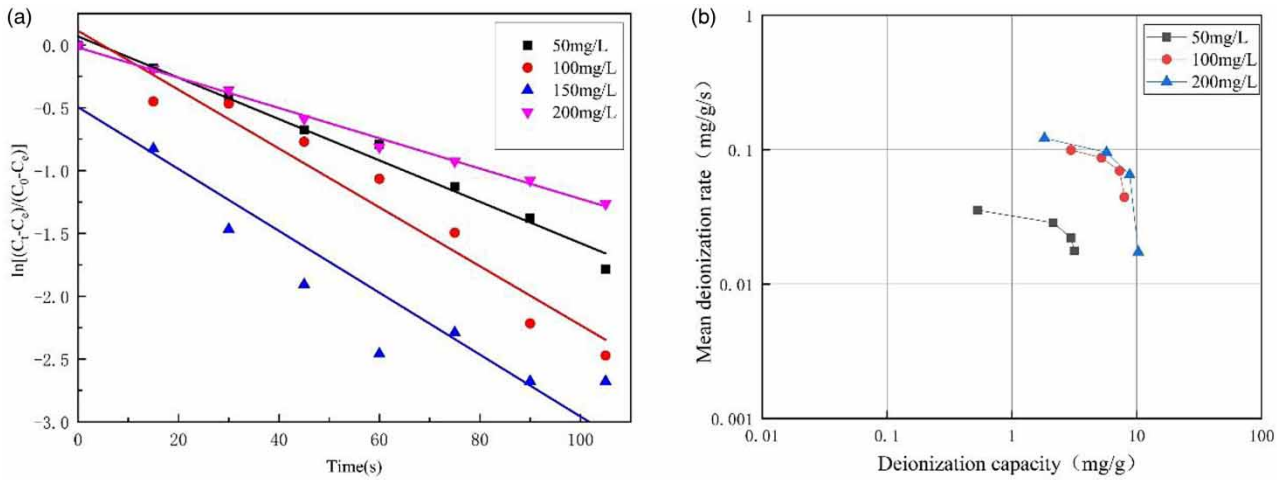

Figure 9 | (a) Pseudo first-order kinetic model linear of 60%T/C composites; (b) CDI Ragone plot of initial salt concentration.

Table 4 | Parameters of each dynamic model

kinetic model	Initial concentration	K-value (s^{-1})	R^2
Pseudo first-order kinetic equation	50	0.0165	0.9849
	100	0.0234	0.9558
	150	0.0246	0.8783
	200	0.0121	0.9946
Pseudo second-order kinetic equation	50	0.0239	0.9805
	100	0.0327	0.8676
	150	0.0446	0.8012
	200	0.0442	0.9427

3.5. DE in actual desulfurization wastewater

The water sample was selected from the desulfurization wastewater of Shenneng power plant in China after triple tank treatment, and had a high concentration of Cl^-. The optimal ratio of TiO_2/CNTs composites (60%T/C) and pure CNTs adsorption material were selected for treatment. After diluting the desulfurization wastewater taken out of the power plant, the experiment was conducted under the conditions of a voltage of 1.2 V and a flow rate of 50 mL/min. Figure 10 shows the DE of 60%T/C composites and pure CNTs adsorption material. It is easy to see from the experimental results that the 60%T/C composites still exhibited excellent performance for DE in the actual desulfurization wastewater treatment.

3.6. The mechanisms for enhanced DE in the CDI with the TiO_2/CNTs anode

In general, the electrosorption process is divided into the following four parts: (i) diffusion of salt ions in brine; (ii) mass transfer of salt ions between the electrode and brine; (iii) electrosorption and energy storage of ions in the electrode bilayer; and (iv) mass transfer of salt ions in the electrode pores (Yin *et al.* 2013). In this experiment, the catalytic mechanism of the TiO_2/CNTs material is shown in Figure 11. Overall, CNTs have a highly conductive support matrix that provides a large surface area for the dispersion of TiO_2 (Xu *et al.* 2020). TiO_2 is a semiconductor material, which makes the material conductive due to the presence of titanium metal and the fact that some electrons can be excited from the valence band to the conduction band driven by thermal energy. The structure of TiO_2 shows that the surface atoms of titanium dioxide nanoparticles are

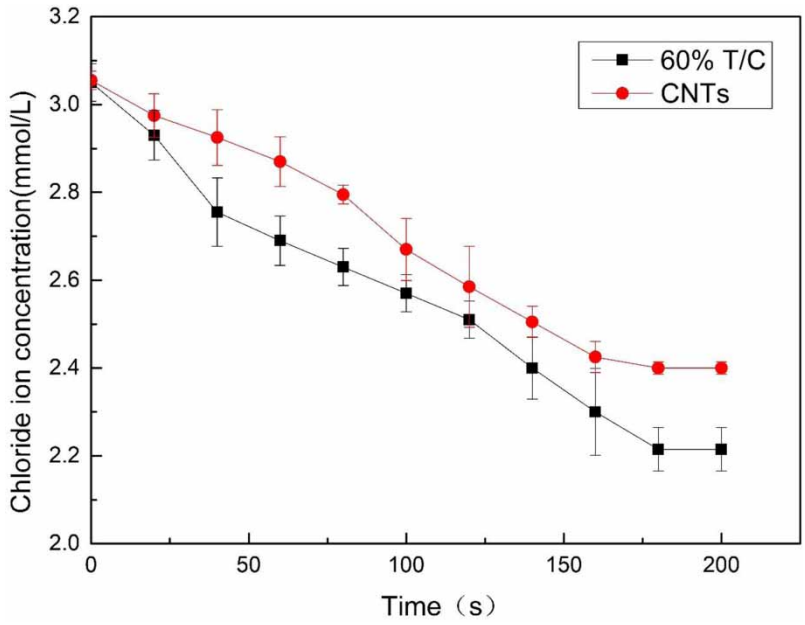

Figure 10 | DE of different materials in desulfurization wastewater.

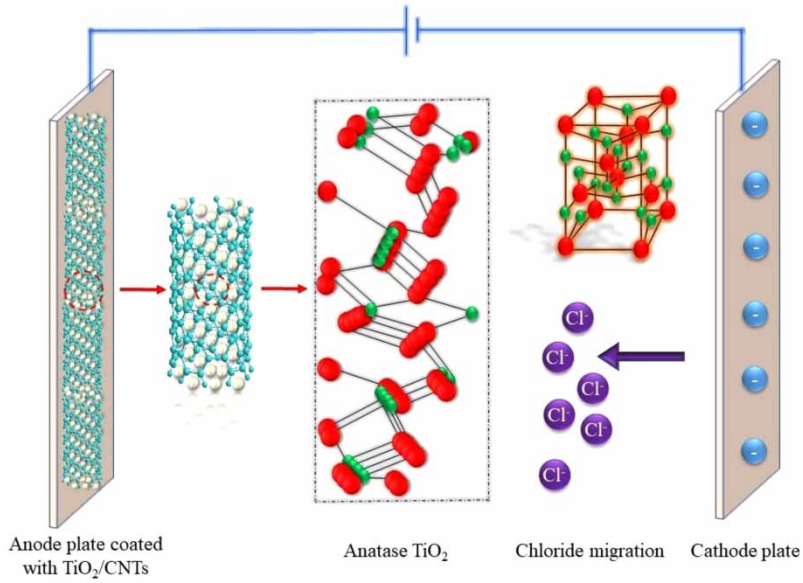

Figure 11 | The catalytic mechanism diagram of the TiO_2/CNTs material.

surrounded by a lack of adjacent, which are unsaturated and are easy for other atoms to combine and stabilize. It is worth noting that the metal cation (Ti^{4+}) on the surface of the material and the positive charge is carried by the electrode that can better attract Cl^- in solution. In addition, large numbers of hydroxyl groups are contained in the surface of the TiO_2 material, which can easily adsorb water and presents hydrophilicity and compensates for the lack of hydrophobicity of CNTs (Tan *et al.* 2020). In summary, it can be seen that the excellent physicochemical and electrochemical properties of TiO_2 accelerate the diffusion of Cl^- to the electrode surface, and Cl^- is eventually adsorbed in the TiO_2/CNTs material. Thereby, enhanced DE is achieved.

4. CONCLUSIONS

In this study, the modification of CDI anode using TiO_2/CNTs composites was proposed for enhancing DE in desulfurization wastewater. The TiO_2/CNTs nanocomposites were successfully prepared by solvothermal method with NMP. SEM and TEM images showing the good dispersion of TiO_2 on the CNTs. Especially in the case of 60%T/C, it showed marked enhancement in wettability and high surface area. The experimental results showed that the maximum specific capacitance of 60%T/C (87.6 F/g) was obtained when the scan rate was 1 mV/s. Whether in NaCl solution or desulfurization wastewater, the maximum adsorption capacity of 60%T/C composites could reach 6.5 mg/g and demonstrated excellent stability. In addition, the experimental results were consistent with the adsorption kinetics analysis. The catalytic and adsorption mechanisms of TiO_2/CNTs were elucidated. In summary, the DE of CDI was significantly improved due to the synergistic effect of TiO_2 and CNTs. The proposed CDI system with TiO_2/CNTs as the anode has a promising application in the dechlorination of desulfurization wastewater.

ACKNOWLEDGEMENT

This work was supported by the financial support of the National Key R&D Program of China (2018YFB0604305-01).

AUTHOR CONTRIBUTION STATEMENT

Shuangcheng Ma, Chang Liu and Lan Ma wrote the main manuscript text, Yongyi Xu and Feng Wang participated in the design of the experiment, and Luyue Hang translated the language of the article.

ADDITIONAL INFORMATION

The manuscript has not been published before or submitted to another journal for the consideration of publication.

COMPETING INTERESTS

The authors declare no competing interests.

DATA AVAILABILITY STATEMENT

All relevant data are included in the paper or its Supplementary Information.

REFERENCES

Boukhalfa, S., Evanoff, K. & Yushin, G. 2012 Atomic layer deposition of vanadium oxide on carbon nanotubes for high-power supercapacitor electrodes. *Energy & Environmental Science* **5**, 6872–6879.

Cheng, Y., Hao, Z., Hao, C., Deng, Y., Li, X., Li, K. & Zhao, Y. 2019 A review of modification of carbon electrode material in capacitive deionization. *RSC Advances* **9**, 2441–24419.

Cong, Y., Li, X., Qin, Y., Dong, Z., Yuan, G., Cui, Z. & Lai, X. 2011 Carbon-doped TiO_2 coating on multiwalled carbon nanotubes with higher visible light photocatalytic activity. *Applied Catalysis. B, Environmental* **107**, 128–134.

Conidi, C., Macedonio, F., Ali, A., Cassano, A., Criscuoli, A., Argurio, P. & Drioli, E. 2018 Treatment of flue gas desulfurization wastewater by an integrated membrane-based process for approaching zero liquid discharge. *Membranes (Basel)* **8**, 117.

Feng, J., Xiong, S. & Wang, Y. 2019 Atomic layer deposition of TiO_2 on carbon-nanotube membranes for enhanced capacitive deionization. *Separation and Purification Technology* **213**, 70–77.

Gaikwad, M. S., Balomajumder, C. & Tiwari, A. K. 2020 Acid treated RHWBAC electrode performance for Cr(VI) removal by capacitive deionization and CFD analysis study. *Chemosphere (Oxford)* **254**, 126781–126781.

Gan, L., Wu, Y., Song, H., Zhang, S., Lu, C., Yang, S., Wang, Z., Jiang, B., Wang, C. & Li, A. 2019 Selective removal of nitrate ion using a novel activated carbon composite carbon electrode in capacitive deionization. *Separation and Purification Technology* **212**, 728–736.

García-Quismondo, E., Santos, C., Soria, J., Palma, J. & Anderson, M. A. 2016 New operational modes to increase energy efficiency in capacitive deionization systems. *Environmental Science & Technology* **50**, 6053–6060.

Gingerich, D. B., Bartholomew, T. V. & Mauter, M. S. 2018a Technoeconomic optimization of emerging technologies for regulatory analysis. *ACS Sustainable Chemistry & Engineering* **6**, 2370–2378.

Gingerich, D. B., Grol, E. & Mauter, M. S. 2018b Fundamental challenges and engineering opportunities in flue gas desulfurization wastewater treatment at coal fired power plants. *Environmental Science Water Research & Technology* **4**, 99–925.

Hafeez, H. Y., Lakhera, S. K., Bellamkonda, S., Rao, G. R., Shankar, M. V., Bahnemann, D. W. & Neppolian, B. 2018 Construction of ternary hybrid layered reduced graphene oxide supported g-C_3N_4-TiO_2 nanocomposite and its photocatalytic hydrogen production activity. *International Journal of Hydrogen Energy* **43**, 3892–3904.

Hassan, A. S. & Darwish, M. A. 2014 Performance of thermal vapor compression. *Desalination* **335**, 41–46.

Hu, C., Hsieh, C., Chen, Y. & Liu, C. 2018 How to achieve the optimal performance of capacitive deionization and inverted-capacitive deionization. *Desalination* **442**, 89–98.

Huang, Z., Yang, Z., Kang, F. & Inagaki, M. 2017 Carbon electrodes for capacitive deionization. *Journal of Materials Chemistry. A, Materials for Energy and Sustainability* **5**, 47–496.

Iaquaniello, G., Salladini, A., Mari, A., Mabrouk, A. A. & Fath, H. E. S. 2014 Concentrating solar power (CSP) system integrated with MED–RO hybrid desalination. *Desalination* **336**, 121–128.

Jande, Y. A. C. & Kim, W. S. 2014 Integrating reverse electrodialysis with constant current operating capacitive deionization. *Journal of Environmental Management* **146**, 463–469.

Jia, F. & Wang, J. 2018 Treatment of flue gas desulfurization wastewater with near-zero liquid discharge by nanofiltration-membrane distillation process. *Separation Science and Technology* **53**, 146–153.

Jia, B. & Zhang, W. 2016 Preparation and application of electrodes in capacitive deionization (CDI): a state-of-art review. *Nanoscale Research Letters* **11**, 1–25.

Kim, T. & Yoon, J. 2013 Relationship between capacitance of activated carbon composite electrodes measured at a low electrolyte concentration and their desalination performance in capacitive deionization. *Journal of Electroanalytical Chemistry (Lausanne, Switzerland)* **704**, 169–174.

Kim, T. & Yoon, J. 2015 CDI ragone plot as a functional tool to evaluate desalination performance in capacitive deionization. *RSC Advances* **5**, 1456–1461.

Kim, K. M., Park, N., Ryu, K. S. & Chang, S. H. 2006 Characteristics of PVdF-HFP/TiO_2 composite membrane electrolytes prepared by phase inversion and conventional casting methods. *Electrochimica Acta* **51**, 5636–5644.

Kim, J., Peck, D., Lee, B., Yoon, S. & Jung, D. 2016 An asymmetrical activated carbon electrode configuration for increased pore utilization in a membrane-assisted capacitive deionization system. *Carbon (New York)* **110**, 521–521.

Lee, B., Park, N., Kang, K. S., Ryu, H. J. & Hong, S. H. 2018a Enhanced capacitive deionization by dispersion of CNTs in activated carbon electrode. *ACS Sustainable Chemistry & Engineering* **6**, 1572–1579.

Lee, S., Kim, Y. & Hong, S. 2018b Treatment of industrial wastewater produced by desulfurization process in a coal-fired power plant via FO-MD hybrid process. *Chemosphere (Oxford)* **210**, 44–51.

Li, H., Ma, Y. & Niu, R. 2016 Improved capacitive deionization performance by coupling TiO_2 nanoparticles with carbon nanotubes. *Separation and Purification Technology* **171**, 93–100.

Liu, P., Chung, L., Shao, H., Liang, T., Horng, R., Ma, C. M. & Chang, M. 2013 Microwave-assisted ionothermal synthesis of nanostructured anatase titanium dioxide/activated carbon composite as electrode material for capacitive deionization. *Electrochimica Acta* **96**, 173–179.

Liu, M., Ding, X., Yang, Q., Wang, Y., Zhao, G. & Yang, N. 2017 A pM leveled photoelectrochemical sensor for microcystin-LR based on surface molecularly imprinted TiO_2@CNTs nanostructure. *Journal of Hazardous Materials* **331**, 309–320.

Liu, N., Sun, S. & Hou, C. 2019 Studying the electrosorption performance of activated carbon electrodes in batch-mode and single-pass capacitive deionization. *Separation and Purification Technology* **215**, 403–409.

Luo, Z., Wang, D., Zhu, D., Xu, J., Jiang, H., Geng, W., Wei, W. & Lian, Z. 2019 Separation of fluoride and chloride ions from ammonia-based flue gas desulfurization slurry using a two-stage electrodialysis. *Chemical Engineering Research & Design* **147**, 73–82.

Ma, S. C., Ma, L., Chen, G. D., Chen, J. N. & Wu, M. F. 2018 Experimental study on desalination using electro-sorption technology with plate-type activated carbon fiber electrode. *Desalination and Water Treatment* **126**, 116–126.

Ma, S. C., Chai, J., Chen, G., Wu, K., Xiang, Y., Wan, Z., Zhang, J., Zhu, H., Kallenborn, R., Becher, G. & Thomassen, Y. 2019 Partitioning characteristic of chlorine ion in gas and solid phases in process of desulfurization wastewater evaporation: model development and calculation. *Environmental Science and Pollution Research International* **26**, 8257–8265.

Moustafa, H. M., Obaid, M., Nassar, M. M., Abdelkareem, M. A. & Mahmoud, M. S. 2020 Titanium dioxide-decorated rGO as an effective electrode for ultrahigh-performance capacitive deionization. *Separation and Purification Technology* **235**, 116178.

Muduli, S., Lee, W., Dhas, V., Mujawar, S., Dubey, M., Vijayamohanan, K., Han, S. & Ogale, S. 2009 Enhanced conversion efficiency in dye-sensitized solar cells based on hydrothermally synthesized TiO_2– MWCNT nanocomposites. *ACS Applied Materials & Interfaces* **1**, 2030–2035.

Nguyen, K. C., Ngoc, M. P. & Nguyen, M. V. 2016 Enhanced photocatalytic activity of nanohybrids TiO_2/CNTs materials. *Materials Letters* **165**, 247–251.

Olowoyo, J. O., Kumar, M., Jain, S. L., Babalola, J. O., Vorontsov, A. V. & Kumar, U. 2019 Insights into reinforced photocatalytic activity of the CNT–TiO_2 nanocomposite for CO_2 reduction and water splitting. *Journal of Physical Chemistry. C* **123**, 367–378.

Porada, S., Zhao, R., Wal, V. D. A., Presser, V. & Biesheuvel, P. M. 2013 Review on the science and technology of water desalination by capacitive deionization. *Progress in Materials Science* **58**, 1388–1442.

Quan, X., Fu, Z., Yuan, L., Zhong, M., Mi, R., Yang, X., Yi, Y. & Wang, C. 2017 Capacitive deionization of NaCl solutions with ambient pressure dried carbon aerogel microsphere electrodes. *RSC Advances* **7**, 35875–35882.

Reddy, R. N. & Reddy, R. G. 2006 Porous structured vanadium oxide electrode material for electrochemical capacitors. *Journal of Power Sources* **156**, 700–704.

Senoussi, H. & Bouhidel, K. E. 2018 Feasibility and optimisation of a batch mode capacitive deionization (BM CDI) process for textile cationic dyes (TCD) removal and recovery from industrial wastewaters. *Journal of Cleaner Production* **205**, 721–727.

Shi, W., Li, H., Cao, X., Leong, Z. Y., Zhang, J., Chen, T., Zhang, H. & Yang, H. Y. 2016 Ultrahigh performance of novel capacitive deionization electrodes based on a three-dimensional graphene architecture with nanopores. *Scientific Reports* **6**, 18966–18966.

Shuangchen, M., Jin, C., Gongda, C., Weijing, Y. & Sijie, Z. 2016 Research on desulfurization wastewater evaporation: present and future perspectives. *Renewable & Sustainable Energy Reviews* **58**, 1143–1151.

Sotto, A., Boromand, A., Balta, S., Kim, J. & Van der Bruggen, B. 2011 Doping of polyethersulfone nanofiltration membranes: antifouling effect observed at ultralow concentrations of TiO_2 nanoparticles. *Journal of Materials Chemistry* **21**, 10311–10320.

Suss, M. E., Porada, S., Sun, X., Biesheuvel, P. M., Yoon, J. & Presser, V. 2015 Water desalination via capacitive deionization: what is it and what can we expect from it? *Energy & Environmental Science* **8**, 2296–2319.

Tan, W., Gao, T. & Wang, Y. 2020 Influence of surface potential on the capacitive performance of the TiO_2 thin-film electrode with different crystalline forms. *Langmuir* **36**, 3836–3842.

Tang, W., Kovalsky, P., Cao, B., He, D. & Waite, T. D. 2016 Fluoride removal from brackish groundwaters by constant current capacitive deionization (CDI). *Environmental Science & Technology* **50**, 10570–10579.

Tian, S., Zhang, Z., Zhang, X. & Ken Ostrikov, K. 2019 Capacitative deionization using commercial activated carbon fiber decorated with polyaniline. *Journal of Colloid And Interface Science* **537**, 247–255.

Wang, Q., Yan, J., Wang, Y., Ning, G., Fan, Z., Wei, T., Cheng, J., Zhang, M. & Jing, X. 2013 Template synthesis of hollow carbon spheres anchored on carbon nanotubes for high rate performance supercapacitors. *Carbon (New York)* **52**, 209–218.

Xing, W., Liang, J., Tang, W., Zeng, G., Wang, X., Li, X., Jiang, L., Luo, Y., Li, X., Tang, N. & Huang, M. 2019 Perchlorate removal from brackish water by capacitive deionization: experimental and theoretical investigations. *Chemical Engineering Journal (Lausanne, Switzerland: 1996)* **361**, 209–218.

Xu, B., Xu, X., Gao, H., He, F., Zhu, Y., Qian, L., Han, W., Zhang, Y. & Wei, W. 2020 Electro-enhanced adsorption of ammonium ions by effective graphene-based electrode in capacitive deionization. *Separation and Purification Technology* **250**, 117243.

Yi, Q., Wang, H., Cong, S., Cao, Y., Wang, Y., Sun, Y., Lou, Y., Zhao, J., Wu, J. & Zou, G. 2016 Self-cleaning glass of photocatalytic anatase TiO_2@Carbon nanotubes thin film by polymer-assisted approach. *Nanoscale Research Letters* **11**, 1–8.

Yin, H., Zhao, S., Wan, J., Tang, H., Chang, L., He, L., Zhao, H., Gao, Y. & Tang, Z. 2013 Three-dimensional graphene/metal oxide nanoparticle hybrids for high-performance capacitive deionization of saline water. *Advanced Materials (Weinheim)* **25**, 6270–6276.

Zhang, Y., Sun, X., Pan, L., Li, H., Sun, Z., Sun, C. & Tay, B. K. 2009 Carbon nanotube–ZnO nanocomposite electrodes for supercapacitors. *Solid State Ionics* **180**, 1525–1528.

Zhang, D., Yan, T., Shi, L., Peng, Z., Wen, X. & Zhang, J. 2012 Enhanced capacitive deionization performance of graphene/carbon nanotube composites. *Journal of Materials Chemistry* **22**, 14696–14704.

Zheng, C., Zheng, H., Yang, Z., Liu, S., Li, X., Zhang, Y., Weng, W. & Gao, X. 2018 Experimental study on the evaporation and chlorine migration of desulfurization wastewater in flue gas. *Environmental Science and Pollution Research International* **26**, 4791–4800.

Zheng, C., Zheng, H., Yang, Z., Liu, S., Li, X., Zhang, Y., Weng, W. & Gao, X. 2019 Experimental study on the evaporation and chlorine migration of desulfurization wastewater in flue gas. *Environmental Science and Pollution Research International* **26**, 4791–4800.

Zhu, Y., Ling, Q., Liu, Y., Wang, H. & Zhu, Y. 2015 Photocatalytic H_2 evolution on MoS_2-TiO_2 catalysts synthesized via mechanochemistry. *Physical Chemistry Chemical Physics: PCCP* **17**, 933–940.

First received 12 March 2021; accepted in revised form 26 July 2021. Available online 9 August 2021